

Stability of Organically Modified Montmorillonites and Their Polystyrene Nanocomposites After Prolonged Thermal Treatment

David J. Frankowski,[†] Michael D. Capracotta,[‡] James D. Martin,[‡] Saad A. Khan,[†] and Richard J. Spontak^{*,†,§}

Departments of Chemical & Biomolecular Engineering, Chemistry, and Materials Science & Engineering, North Carolina State University, Raleigh, North Carolina 27695

Received August 19, 2006. Revised Manuscript Received March 15, 2007

Melt intercalation of montmorillonite (MMT) into polymeric matrices to improve the mechanical properties of polymers has evolved into a subject of tremendous fundamental and technological interest. The thermal treatment experienced during processing or end use can substantially affect the clay and diminish the target properties of polymer/clay nanocomposites (NCs) because of deintercalation or degradation of surface modifiers. In this work, changes in morphology, chemistry, and thermal stability of organically modified (OM) MMT after annealing in O₂-rich and N₂ environments are investigated. Degradation of the alkyl ammonium cation occurs at temperatures as low as 105 °C upon prolonged exposure in an O₂-rich environment. X-ray diffractometry (XRD) performed in situ establishes the response of two OM-MMTs to elevated temperatures at short times, whereas ex situ XRD provides insight into high-temperature exposure at long times. Active sites on the silicate surfaces are found to induce scission of, as well as chemical interaction with, the chains comprising a polystyrene (PS) matrix. Size-exclusion chromatography indicates that PS chain scission occurs primarily after relatively short annealing times, whereas branching and cross-linking are more prevalent after long exposure times in an O₂-rich environment.

1. Introduction

Nanoscale dispersion of inorganic fillers in a polymeric matrix can be achieved by using layered silicates, e.g., montmorillonite (MMT), that are rendered organophilic via cation exchange of the native Na⁺ ion for alkyl ammonium ions. Cation exchange can also reduce silicate–silicate interactions, thereby facilitating platelet separation. Immiscible, intercalated, exfoliated, and mixed morphologies are common structural classifications that reflect interactions between the component species (i.e., the polymer, silicate, and alkyl ammonium cation) and the nanocomposite (NC) fabrication process.^{1–4} Immiscible NCs, or microcomposites, possess well-ordered clay platelets with a lamellar (*d*) spacing similar to that of the neat clay. Intercalated NCs exhibit a *d*-spacing that is larger relative to the pristine clay and may be further categorized as disordered or flocculated. Exfoliated NCs typically show evidence of disordered single platelets (with no discernible lamellar spacing) uniformly dispersed throughout the polymeric matrix. Three general strategies developed to produce intercalated or exfoliated NCs are in

situ polymerization and solvent or melt intercalation. The NCs generated via in situ polymerization may be thermally treated to ensure desired reaction conversion, thermal stability, or orientation. Thermal treatment of exfoliated poly(methylmethacrylate)^{5,6} and polyamide (PA)⁷ NCs prepared by in situ polymerization can induce aggregation of the clay platelets wherein penetrated polymer chains are expelled from the galleries to yield a mixed morphology composed of intercalated and exfoliated platelets. Melt-fluxing tends to promote greater chain expulsion than static annealing. Although Huang and Brittain⁶ have shown that clays modified with tethered polymer chains can better preserve exfoliated morphologies formed during in situ polymerization, a more rational approach to designing thermally stable NCs is to understand the relevant molecular-level processes involved to avoid destabilization.

Melt intercalation constitutes a preferable fabrication route because it is environmentally benign (avoiding the use of organic solvents), successful for more polymer–clay combinations than other intercalation strategies, and scalable to meet industrial needs. In melt intercalation, the polymer and clay are heated above the glass-transition temperature (*T_g*) of the polymer either quiescently or under shear as in extrusion. It is well-known and intuitively expected that annealing organically modified montmorillonite (OM-MMT) progressively degrades the alkyl surfactants and collapses

* To whom correspondence should be addressed. E-mail: rich_spontak@ncsu.edu.

[†] Department of Chemical & Biomolecular Engineering, North Carolina State University.

[‡] Department of Chemistry, North Carolina State University.

[§] Department of Materials Science & Engineering, North Carolina State University.

- (1) Giannelis, E. P. *Adv. Mater.* **1996**, *8*, 29.
- (2) Krishnamoorti, R.; Yurekli, K. *Curr. Opin. Colloid Interface Sci.* **2001**, *6*, 464.
- (3) Ray, S. S.; Okamoto, M. *Prog. Polym. Sci.* **2003**, *28*, 1539.
- (4) Zanetti, M.; Lomakin, S.; Camino, G. *Macromol. Mater. Eng.* **2000**, *279*, 1.

(5) Tabtiang, A.; Lumlong, S.; Venables, R. A. *Polym.–Plast. Technol. Eng.* **2000**, *39*, 293.

(6) Huang, X. Y.; Brittain, W. J. *Macromolecules* **2001**, *34*, 3255.

(7) Morgan, A. B.; Gilman, J. W. *J. Appl. Polym. Sci.* **2003**, *87*, 1329.

Table 1. Molecular Weights upon Annealing PS and NC7 at 250 °C in an O₂-Rich Environment

clay content (wt %)	annealing time (h)	overall			peak 1 ^a			peak 2 ^a		
		<i>M_n</i> (kDa)	<i>M_w</i> (kDa)	<i>M_w/M_n</i>	<i>M_n</i> (kDa)	<i>M_w</i> (kDa)	<i>M_w/M_n</i>	<i>M_n</i> (kDa)	<i>M_w</i> (kDa)	<i>M_w/M_n</i>
0	0	215	330	1.4						
0	0.1 ^b	173	263	1.5						
0	3.75	96	202	2.1	149	229	1.5	29	31	1.1
0	6.5	25	107	4.2	117	180	1.5	13	16	1.3
0	14	99	212	2.2	181	255	1.4	34	38	1.1
0	24	150	174	1.2	160	212	1.3	146	153	1.1
7	0	173	267	1.5						
7	3.5	114	170	1.5	147	213	1.5	77	78	~1.0
7	14	110	206	1.9	119	227	1.9	74	75	~1.0
7	28	198	236	1.2	171	212	1.2	260	275	1.1
7	38	254	350	1.4	174	199	1.1	410	473	1.2

^a Values are omitted when only one peak is present. ^b PS after extrusion (185° die/melt temperature, ~0.1 h residence time).

the platelets.^{8–11} Xie et al.¹² have proposed, however, that annealing clay may conversely increase platelet separation because of increased pressure inside the interlayer after the organic surfactant decomposes. Whether such degradation is beneficial prior to, or during, melt intercalation remains uncertain. Ex situ X-ray diffractometry (XRD) performed by Yoon et al.¹³ corroborates that the OM-MMT Cloisite 15A (C15A) expands upon annealing at 250 °C, but only at relatively short times (<10 min). The purpose of the present study is to ascertain the effects of high-temperature oxidative environments on the clay, polymer, and daughter NC and thus resolve conflicting reports by systematically varying the clay, as well as annealing temperature, atmosphere, and time. To address these issues, we employ a series of complementary analyses using Fourier transform infrared (FTIR) spectroscopy, XRD, and size-exclusion chromatography (SEC). We also examine XRD and SEC results that can be misinterpreted when assessing (i) the existence or extent of clay intercalation from Bragg–Brentano reflection data and (ii) (catalytic) degradation of polymer/clay NCs.

II. Experimental Section

A. Materials. Polystyrene (PS) 1300 with number- and weight-average molecular weights (in kDa, see Table 1) of 215 (*M_n*) and 330 (*M_w*) was kindly supplied in pellet form by Nova Chemicals (Calgary, Alberta, Canada). Natural and organically modified Cloisite clays were acquired from Southern Clay Products (Gonzales, TX). Cloisite Na⁺ (CNa⁺) is a natural MMT, whereas Cloisite 10A (C10A) and Cloisite 15A (C15A) are OM-MMTs containing quaternary ammonium salts: dimethyl benzyl hydrogenated tallow for C10A and dimethyl dihydrogenated tallow for C15A (see Figure 1). The cation exchange capacity (CEC) of CNa⁺, C10A, and C15A are reported by the supplier as 93, 125, and 125 mequiv/100 g of clay, respectively. Alkanox 240, an organophosphite antioxidant, was provided by Chemtura Corp. (Middlebury, CT). High-performance liquid chromatography (HPLC) grade tetrahydrofuran (THF), and toluene for SEC were obtained from Acros Organics (Morris Plains, NJ) and used as-received.

B. Specimen Preparation. The C15A was dried overnight in a vacuum oven before compounding. A 19 mm single-screw extruder (Wayne Machine & Die Co., Wayne, NJ) with a length/diameter (*L/D*) ratio of 30/1 and equipped with a Saxton mixing section at its end was used for this purpose. Formulations with C15A at concentrations of 7 or 17 wt % (hereafter referred to as NC7 or NC17, respectively) were prepared by dry blending PS pellets, clay, and 0.6 wt % stabilizer in glass jars for 5 min prior to addition to the hopper. Samples were extruded at 50 rpm through the bore possessing a temperature profile (in °C) of 140/175/180/185. The adapter and die temperatures were both maintained at 185 °C. Discs for rheometry were melt-pressed at 175 °C in circular molds varying in thickness and diameter (8, 10, or 25 mm). Once pressed, the molds were quenched in water at 10–20 °C.

C. Specimen Characterization. The FTIR analyses were performed on a Nicolet Magna-IR 750 spectrophotometer with 256 scans acquired at a resolution of 4 cm⁻¹. A DTGS KBr detector with a KBr beam splitter was employed, and background spectra were collected before each sample. Clay films were prepared by first mixing KBr and clay at an approximate 40:1 mass ratio and then pressing the mixture in a circular die at ambient temperature and 3 MPa. The NCs were scanned without KBr after melt pressing.

Ex situ XRD was performed on an Inel XRG 3000 diffractometer (Artenay, France) with Cu Kα radiation ($\lambda = 0.154$ nm) at 35 kV and 30 mA. Specimens were subjected to a variety of thermal annealing conditions in open crucibles prior to XRD analysis at ambient temperature. Measurements were conducted in reflection mode using the Bragg–Brentano parafocusing geometry (powders and films) and transmission mode by loading powder into 0.3–0.7 mm glass capillary tubes purchased from the Charles Supper Co. (Natick, MA) and calibrated to an external silicon standard. The incidence angle was maintained at ~4° in reflection experiments except when the effect of preferred clay orientation was investigated. In this case, the incidence angle was rotated from grazing to 90°. To obtain structural data free of preferred orientation, powdered samples were loaded into the capillary tubes mounted on a rotating goniometer for measurement in transmission mode.

Variable-temperature powder XRD was likewise performed in situ on the National Synchrotron Light Source beamline X7b ($\lambda = 0.0921$ nm) at Brookhaven National Laboratory. Diffraction patterns were acquired using Debye–Scherrer collimation and a MAR345 image plate detector system. Samples were placed in 0.5–0.7 mm glass capillaries and sealed to prevent escape of volatile decomposition products. Capillaries were mounted on a rotating goniometer head and the temperature was controlled by a forced air furnace. The temperature was increased at a rate of 25 °C/min, and XRD patterns were collected every 1 min. In a typical experiment, a sample was exposed to the synchrotron X-ray beam for 20 s, and

- (8) Wang, Z. M.; Chung, T. C.; Gilman, J. W.; Manias, E. J. *Polym. Sci., Part B: Polym. Phys.* **2003**, *41*, 3173.
 (9) Dharaiya, D.; Jana, S. C. *Polymer* **2005**, *46*, 10139.
 (10) Lim, Y. T.; Park, O. O. *Rheol. Acta* **2001**, *40*, 220.
 (11) Lee, J. W.; Lim, Y. T.; Park, O. O. *Polym. Bull.* **2000**, *45*, 191.
 (12) Xie, W.; Gao, Z. M.; Pan, W. P.; Hunter, D.; Singh, A.; Vaia, R. *Chem. Mater.* **2001**, *13*, 2979.
 (13) Yoon, P. J.; Hunter, D. L.; Paul, D. R. *Polymer* **2003**, *44*, 5323.

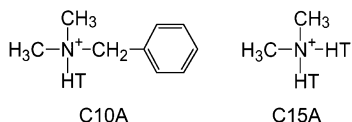


Figure 1. Alkyl ammonium cations in C10A and C15A, where HT denotes a hydrogenated tallow chain consisting of the following *n*-alkanes: C₁₄ (3.5%), C₁₅ (0.5%), C₁₆ (31.0%), C₁₇ (1.0%), and C₁₈ (61.0%), as well as 3.0% C₁₈ containing one double bond and 16 single bonds.

the image plate was read during the subsequent 40 s prior to the next scan, thereby resulting in a change in specimen temperature of ~ 8 °C for each XRD dataset (hereafter labeled with the starting temperature). Neat clays were annealed at 105 °C for 12–24 h to remove adsorbed water prior to XRD analysis.

A DAWN multi-angle light scattering (MALS) detector and Optilab DSP interferometric refractometer from Wyatt Technology Corp. (Santa Barbara, CA), along with a Waters 2950 HPLC injection system from Waters Corp. (Milford, MA), were used to measure molecular weight distributions of PS and PS/OM-MMT NCs under widely varying conditions. Most SEC runs were performed at 0.5 mL/min in THF with Styragel HR4 and HR4E columns, also from Waters Corp. Additional systems employed for molecular weight determination were a (i) Waters 2695 HPLC unit with μ Styragel columns (pore sizes of 1×10^4 , 1×10^3 , and 1×10^2 nm) and THF at 1.0 mL/min using a Waters 410 refractometer and both a universal calibration curve and a MALS detector, and (ii) a Waters 2960 HPLC unit with Styragel HR4, HR4E, and HR3 columns and toluene at 0.3 mL/min using a miniDAWN and Optilab rEX. All elutions were performed at 25 °C.

III. Results and Discussion

A. Chemical Characteristics. Montmorillonite-based clays are hydrophilic materials by their very nature and as such must be dried before compounding to remove bound water. If a surface-modified clay changes under such conditions or, alternatively, over time at storage or application conditions, expected properties may be stochastically skewed without prior knowledge. In this section, we address the issue of OM-MMT thermal stability by annealing CNa⁺, C10A, and C15A in air at 105 and 160 °C and periodically removing specimens for FTIR analysis. The initial FTIR spectra for CNa⁺, PS, NC7, and C15A, as well as the spectrum for C15A after annealing in air at 160 °C for 39 days, are displayed in Figure 2, and corresponding peak assignments before and after annealing at 105 °C for 45 days or 160 °C for 39 days are summarized in Table 2. Note that some of the peaks are not visible in Figure 2 because of the scaling of the absorbance axis. In the CNa⁺ spectrum, Al–O stretching and Si–O bending are observed at 466, 524, and 625 cm^{-1} . The first two peaks are shifted to 463 and 521 cm^{-1} and the third peak remains at 625 cm^{-1} in the spectrum for C15A and C10A annealed at 105 °C. Note that the peak at 521 cm^{-1} shifts to 523 cm^{-1} (closer to the peak for CNa⁺) after prolonged annealing at 160 °C, indicating that the organic surfactants influence the vibrations of the inorganic elements comprising the silicate sheets. The FTIR spectrum obtained from C15A also exhibits a single peak at 721 cm^{-1} , which arises from $(\text{CH}_2)_n$ (where *n* is the number of repeat methylene units and must be greater than 4 for this peak to become evident) rocking absorption. The spectrum of C10A displays two peaks at 702 and 730 cm^{-1} , with the latter being

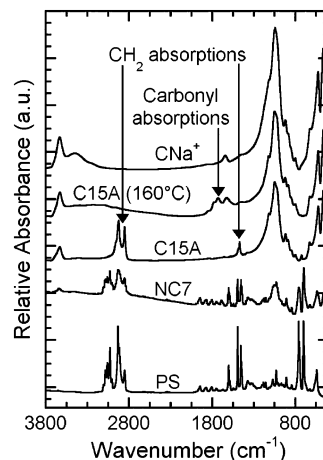


Figure 2. FTIR spectra collected from pristine CNa⁺, C15A, PS, and NC7, as well as C15A after annealing at 160 °C in an O₂-rich environment for 39 days (labeled, along with key absorption bands).

broad and likely a convolution of $(\text{CH}_2)_n$ rocking and CH phenyl ring substitution band (760 cm^{-1}) absorptions. The peak at 702 cm^{-1} is also due to CH phenyl ring substitution band absorption. All three hydrocarbon peaks (702, 721, and 730 cm^{-1}) disappear after annealing at 160 °C because of thermal degradation of the hydrogenated tallow (HT) units and phenyl moieties.

At 798, 844–846, 885, and 917 cm^{-1} , the three pristine clays possess common low-intensity peaks that arise from bending vibrations among the metal elements and a hydroxyl unit, although we recognize that these peaks may reflect small concentrations of quartz or kaolinite present in CNa⁺ after mining and purification. The spectrum acquired for CNa⁺ exhibits a peak at ~ 1042 cm^{-1} , whereas the organically modified clays display a peak at 1048 cm^{-1} and a soft shoulder at 1024 cm^{-1} . Unlike the 523 cm^{-1} peak discussed above, however, the 1048 cm^{-1} peak does not shift after annealing at 160 °C. A second peak corresponding to Si–O stretching for the modified clays is located at 1117 cm^{-1} , but shifts to higher wavenumbers after annealing at both 105 °C (1119 cm^{-1}) and 160 °C (1121 cm^{-1}). In contrast, CNa⁺ has a thermally stable peak in the vicinity of 1121 cm^{-1} . The shift of the peaks observed in the spectra of the modified clays upon annealing indicates that (i) alkyl ammonium cation exchange affects Si–O stretching, and (ii) degradation of the alkyl ammonium cations occurs at temperatures as low as 105 °C. Peaks positioned at 1378 and 1418 cm^{-1} in the spectra for both C10A and C15A reflect CH₃ deformation absorption and disappear after annealing at 160 °C. Peaks between 1450 and 1500 cm^{-1} are attributed to CH₂ bending vibration and likewise disappear after annealing at 160 °C. The 1636 cm^{-1} peak, assigned to bound water and H–O–H bending vibration, is less intense for the modified clays than for CNa⁺, which is consistent with the former being less hydrophilic than CNa⁺. Retention of this peak (albeit slightly shifted) after annealing at 160 °C confirms that the water is strongly bound. Although carbonyl peaks form between 1700 and 1800 cm^{-1} for all clays after annealing at 160 °C, the modified clays form low-intensity carbonyl peaks at ~ 1702 cm^{-1} after annealing at only 105 °C, thus establishing that

Table 2. FTIR Peaks of Natural and Modified MMT before and after Annealing at 160 °C for 39 day

absorption modes	CNa ⁺	CNa ⁺ (160 °C)	C10A	C10A (160 °C)	C15A	C15A (160 °C)
Al–O stretching and Si–O bending	466, 524, 625	466, 524, 625	463, 521, 625	463, 523, 625	463, 521, 625	463, 523, 625
CH phenyl ring substitution	n/a	n/a	702	n/a	n/a	n/a
(CH ₂) _n rocking	n/a	n/a	730 ^a	n/a	721	n/a
Si–O stretching	1121	1121	1117	1121	1117	1121
CH ₃ deformation	n/a	n/a	1378, 1418	n/a	1378, 1418	n/a
CH ₂ bending	n/a	n/a	1450–1500	n/a	1450–1500	n/a
Carbonyl groups	n/a	1701	n/a	1719, 1772 ^b	n/a	1724, 1773 ^b
CH ₂ symmetric stretching	n/a	n/a	2850	n/a	2850	n/a
CH ₂ asymmetric stretching	n/a	n/a	2922	n/a	2922	n/a
CH aromatic ring	n/a	n/a	3034, 3064	n/a	n/a	n/a

^a Broad peak probably corresponding to peaks at ~735 (phenyl ring substitution) and ~720 cm⁻¹ (CH₂ rocking). ^b Peak at 1701 cm⁻¹ grows after annealing at 105 °C.

105 °C is sufficient to initiate degradation of the alkyl ammonium cations.

The two modified clays exhibit intense peaks at 2850 and 2922 cm⁻¹ due to CH₂ symmetric and asymmetric stretching, respectively. These peaks vanish after annealing at 160 °C, indicating that the HT chains decompose into volatile molecules. The disappearance of CH₂-related vibrations has also been observed¹⁴ after heating a MMT modified with stearyltrimethyl ammonium chloride to 500 °C, although lower annealing temperatures were not examined. Previous gas chromatography and mass spectrophotometry studies^{12,15} verify that alkanes, alkenes, and amines are produced by thermal decomposition at temperatures considered in our study. The normal boiling points of *n*-alkanes vary between -161 °C (methane, C₁) and 317 °C (octadecane, C₁₈). The dissociation energy is lowest for C–N bonds, in which case toluene and the HT chains are most likely released first. Random scission of CH₂–CH₂ bonds subsequently fragments HT chains into shorter alkane molecules that immediately vaporize, leaving behind only longer alkanes for continued scission.^{16,17} The two peaks at 3034 and 3064 cm⁻¹ in the C10A spectrum are also attributed to the phenyl ring (CH aromatic ring absorption). These peaks persist upon annealing at 105 °C, but disappear when the clay is annealed at 160 °C. The peaks located at 3430–3440 and 3630 cm⁻¹ for all clays are due to OH stretching from lattice water coupled with octahedral cations. As with the peak identifying bound water at 1636 cm⁻¹, these peaks also remain after annealing at 160 °C. Thus, the characteristic inorganic vibrations of CNa⁺ do not substantially shift after organic cation exchange or annealing. The disappearance of peaks corresponding to hydrocarbon vibrations, e.g., (CH₂)_n rocking, CH₃ deformation, CH aromatic ring, and CH₂ bending and stretching, is complete after annealing for 45 days in air at 160 °C. Carbonyl formation is, however, detected at significantly lower temperatures (105 °C) and may indicate defects within the layers, weak links in the alkyl surfactant, or free surfactant that is less thermally stable.

Paul and co-workers^{18,19} have explored the occurrence of extrusion-induced color changes in polycarbonate (PC) and

nylon NCs by colorimetry and UV–vis spectrophotometry. Increasing the concentration of clay in PC NCs progressively turns the samples from off-white to brown, with high-molecular-weight PC displaying more coloration than low-molecular-weight PC.¹⁹ Long residence times produce more coloration and even black nylon NCs for those clays prone to thermal degradation.¹⁸ Here, we qualitatively describe coloration trends for both clays and their PS NCs upon annealing between 105 and 250 °C. The initial color of the clays is off-white, but CNa⁺ becomes increasingly darker and slightly tan when annealed in air above 150 °C. Annealing C10A or C15A in air at 105 °C changes the color to light tan after 10 days and then light brown after 45 days. Annealing these clays in air at 160 °C results in brown coloration after 39 days, whereas annealing at 200 °C causes the color to change to light gray within 1 min of exposure. After 5 min at 200 °C, the color darkens, eventually becoming dark gray for C10A and black for C15A. The darker color for C15A is consistent with previous results^{18,19} and suggests that greater carbon residue remains trapped within the clay. Residues from thermogravimetric analysis (TGA) reveal that annealing in N₂ up to 1000 °C results in both pristine and previously annealed (at 105 or 160 °C) (i) CNa⁺ to turn brown, (ii) C10A to turn dark gray, and (iii) C15A to turn black.

The PS NCs after extrusion appear light tan, and subsequent specimen annealing above 105 °C promotes further coloration, although to a less-pronounced extent than for the exchanged clay. Whereas annealing C15A in air at 200 °C for 0.2 h is sufficient for C15A to turn black, the NCs require ~10 h at 250 °C to achieve similar coloration. The onset degradation temperature discerned by TGA performed under N₂ for C15A is significantly lower relative to the NCs (~180 vs ~270 °C), indicating that higher temperatures or longer annealing times are necessary for the NCs to undergo comparable surfactant decomposition as pristine clay in oxidative or inert environments. This observation is consistent with the findings of several studies^{20–26} that report

- (14) Hwu, J.; Jiang, G. J.; Gao, Z. M.; Xie, W.; Pan, W. P. *J. Appl. Polym. Sci.* **2002**, *83*, 1702.
 (15) Edwards, G.; Halley, P.; Kerven, G.; Martin, D. *Thermochim. Acta* **2005**, *429*, 13.
 (16) Sanderson, R. T. *Chemical Bonds and Bond Energy*; Academic Press: New York, 1971; Vol. 21.
 (17) *Lange's Handbook of Chemistry*, 15th ed.; McGraw-Hill: New York, 1999.

- (18) Yoon, P. J.; Hunter, D. L.; Paul, D. R. *Polymer* **2003**, *44*, 5341.
 (19) Fornes, T. D.; Yoon, P. J.; Paul, D. R. *Polymer* **2003**, *44*, 7545.
 (20) Vyazovkin, S.; Dranca, I.; Fan, X. W.; Advincula, R. *J. Phys. Chem. B* **2004**, *108*, 11672.
 (21) Vyazovkin, S.; Dranca, I.; Fan, X. W.; Advincula, R. *Macromol. Rapid Commun.* **2004**, *25*, 498.
 (22) Bourbigot, S.; Gilman, J. W.; Wilkie, C. A. *Polym. Degrad. Stab.* **2004**, *84*, 483.
 (23) Qin, H. L.; Zhang, S. M.; Zhao, C. G.; Feng, M.; Yang, M. S.; Shu, Z. J.; Yang, S. S. *Polym. Degrad. Stab.* **2004**, *85*, 807.

degradation temperatures decrease by 50–150 °C when OM clays are annealed in air instead of N₂. Although the possibility that embedding organically modified clays in a polymer can protect the alkyl surfactants at elevated temperatures deserves additional attention, analysis of the FTIR spectrum acquired from NC7 is hindered by the presence of commercial additives used during or after polymerization, as well as overlapping vibrations of the polymer and alkyl surfactants. It is therefore not surprising that the spectrum of NC7 before annealing (see Figure 2) is a convolution of the spectra collected from neat PS and annealed C15A (at 105 °C). Some of the peaks in the spectrum for NC7 are observed to increase in intensity and breadth upon annealing, suggesting that chemical changes occur at elevated temperatures.

B. Morphological Characteristics. *In Situ* XRD. Synchrotron XRD patterns of C15A and C10A, collected *in situ* as a function of temperature, are presented in panels a and b, respectively, of Figure 3. Note that the XRD pattern corresponding to CNa⁺ is not shown as it does not change with increasing temperature up to 275 °C, indicating that the stacking of the silicate sheets is thermally stable, which is consistent with the FTIR data discussed above. Each of the clays exhibit two broad diffraction features at approximately 1.5° and 3° 2θ ($\lambda = 0.092$ nm), though the relative intensities of these signatures are distinct for each clay. The possibility that these peaks represent different orders of lamellar spacings (i.e., 001 and 002) is ruled out on the basis of their divergent behavior upon heating: the low-angle peak shifts to lower angles, whereas the high-angle peak shifts to higher angles. Instead, the existence of these two diffraction peaks is attributed to a bimodal distribution of clay layers due to incomplete exchange of Na⁺ for quaternary ammonium cations, even though the CECs of both modified clays are 125 mequiv/100 g of clay (whereas that of CNa⁺ is 93 mequiv/100 g of clay). Gelfer et al.²⁷ have demonstrated that structural heterogeneities of minerals can render some layers almost completely devoid of organic surfactant and others with excess surfactant at or below the CEC of the natural clay. Independent studies suggest that 5–15% of the platelets may retain Na⁺ cations during cation exchange.¹² In the case of C15A, a low-intensity peak corresponding to a *d*-spacing of 1.64 nm is observed to shift to 1.57 nm as the temperature is increased, corroborating partial thermal degradation of the alkyl surfactant. The principal scattering peak in the XRD pattern of C15A corresponds to a *d*-spacing of 3.16 nm, which increases slightly (3.30 nm) with increasing temperature up to 125 °C and then stabilizes. Interestingly, 10 min after the temperature reaches ~275 °C, the *d*-spacing further increases to 3.49 nm. Because the capillary containing the *in situ* heated specimen is sealed, any degradation products from the organic sur-

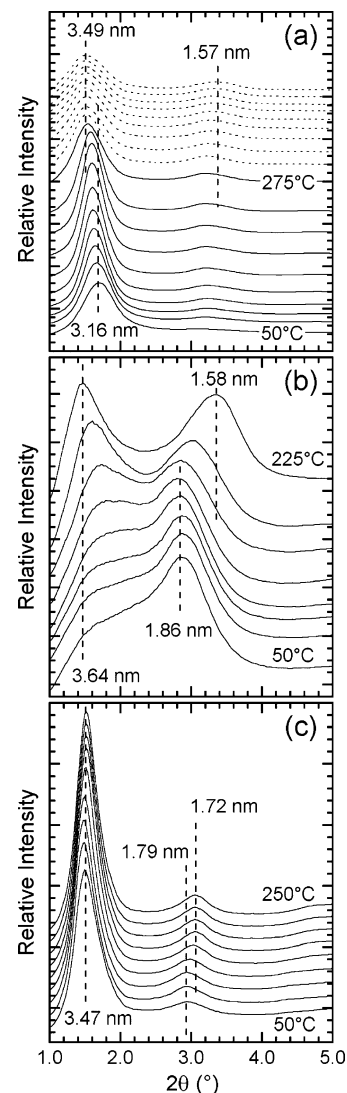


Figure 3. *In situ* XRD patterns ($\lambda = 0.092$ nm) acquired from (a) C15A, (b) C10A, and (c) NC17. The heating rate was ~25 °C/min, and datasets were acquired every minute. (a) Temperature was held constant after reaching 275 °C (indicated by dotted lines) for 9 min while isothermal data were collected every minute.

factant remain trapped inside the capillary. Such degradation species include alkanes that interact favorably with methyl and methylene groups residing in the galleries of undegraded clay particles. A pressure buildup due to such species intercalated inside the galleries as proposed previously¹² is a reasonable mechanism to explain *d*-spacing increases during thermally induced surfactant degradation.

The XRD pattern for C10A displayed in Figure 3b possesses an initial scattering reflection located at 1.86 nm, which corresponds to silicate layers with aromatic cations contained in the galleries. The initial pattern also shows a shoulder at low 2θ (1.5–2.0°), which signifies a *d*-spacing of 2.65–3.50 nm. At temperatures up to 175 °C, the low-angle shoulder progressively increases in intensity to become a clearly discernible scattering peak. Although the reason for the presence of this low 2θ reflection is uncertain, the similarity to C15A indicates that some of the quaternary ammonium cations in C10A may begin as (because of contamination) or evolve into (because of thermal degradation) simple, short-chain alkanes within the clay galleries. The broadness of this shoulder at low temperature and its

(24) Gianelli, W.; Ferrara, G.; Camino, G.; Pellegatti, G.; Rosenthal, J.; Trombini, R. C. *Polymer* **2005**, *46*, 7037.

(25) Ramos, F. G. R.; Melo, T. J. A.; Rabello, M. S.; Silva, S. M. L. *Polym. Degrad. Stab.* **2005**, *89*, 383.

(26) Qi, R. R.; Jin, X.; Nie, J. H.; Yu, W.; Zhou, C. X. *J. Appl. Polym. Sci.* **2005**, *97*, 201.

(27) Gelfer, M.; Burger, C.; Fadeev, A.; Sics, I.; Chu, B.; Hsiao, B. S.; Heintz, A.; Kojo, K.; Hsu, S. L.; Si, M.; Rafailovich, A. *Langmuir* **2004**, *20*, 3746.

sharpening with elevated temperature further suggest that this larger feature is not well-ordered at ambient temperature, but structurally refines with increasing temperature. Between 175 and 200 °C, the two peaks begin to significantly diverge, with the low-angle peak moving to lower angle (increasing the d -spacing to 3.64 nm at 225 °C) and the high-angle peak moving to higher angle (decreasing the d -spacing to 1.58 nm at 225 °C). The mechanism responsible for this high-temperature structural evolution is believed to be the same as for C15A, i.e., degradation of the surfactant and intercalation of the vaporized alkane and phenyl moieties into the clay galleries. Three features warrant comparison between the high-temperature responses of C10A and C15A: (i) collapse and intercalation of C10A platelets occurs at lower temperature than for C15A (200 vs 275 °C); (ii) collapsed platelets of C15A and C10A reach the same d -spacing of ~ 1.58 nm, which is expected because the cations differ only in replacement of one of the HT chains for toluene (which likely cleaves off at the $C_6H_5CH_2-N$ or $C_6H_5-CH_2N$ bond),^{16,17} and (iii) the low 2θ peaks for C10A and C15A shift to higher, but different, d -spacings (3.64 vs 3.49 nm), which reflects the difference between bulky phenyl rings and alkane chains re-intercalated as volatile compounds within the clay galleries.

The XRD pattern presented in Figure 3c for NC17 initially exhibits two discernible reflections at 2.94 and 1.49° 2θ , corresponding to d -spacings of 1.79 and 3.47 nm, respectively. It is important to recognize that after extrusion, the C15A particles in NC17 possess a more complex thermal and stress history, in which case direct comparison with the data for neat C15A may not be possible. On the basis of the measured d -spacings, however, comparison with C15A at ca. 200 °C (~ 1.7 and ~ 3.4 nm) appears to be the most reasonable. The low-intensity, high- 2θ peak for NC17 is observed to shift to higher 2θ (a smaller d -spacing) with increasing temperature. This d -spacing is larger for NC17 than for C15A, thereby corroborating that the clay is less susceptible to thermal degradation when it is embedded in a polymeric matrix. The principal scattering peak at low 2θ for NC17 is indicative of an intercalated NC. Although the position of this peak does not change appreciably with increasing temperature, we present evidence in the next section that this morphology is thermally unstable.

Ex Situ XRD. As mentioned in the previous section, XRD patterns acquired in situ from CNa⁺ are not provided because the d -spacing remains virtually unchanged up to the maximum temperature of 275 °C (reached in 11 min). Specimens annealed in an oven and measured ex situ by XRD permit assessment of structural changes after considerably longer heat treatments. Since the X-ray wavelengths employed by the two diffractometers differ, the 2θ peak positions in Figures 3 and 4 cannot be directly compared, but the corresponding d -spacings can. Interestingly, Figure 4a reveals that after relatively long exposure times (37 days) at 160 °C the lamellar diffraction peak for the CNa⁺ clay severely broadens to higher 2θ , suggesting a significant loss of order (or decrease in grain size) and an accompanying decrease in d -spacing by $\sim 8\%$. This decrease in d -spacing is attributed to Na⁺ cations being replaced with protons. Although a

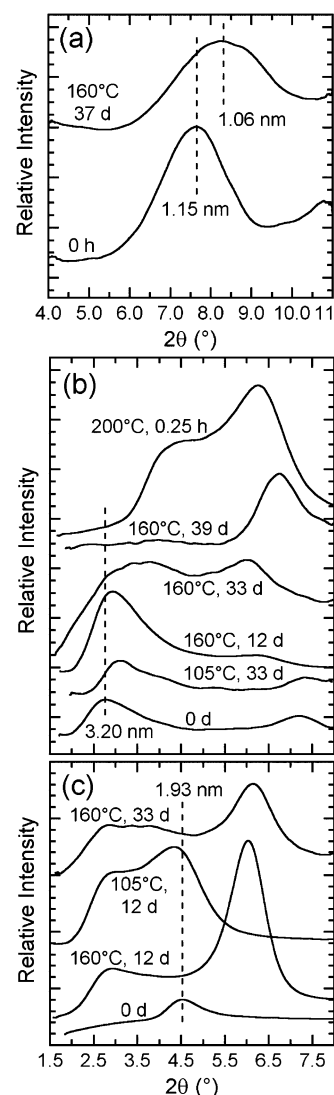


Figure 4. Ex situ XRD patterns ($\lambda = 0.154$ nm) obtained from (a) CNa⁺, (b) C15A, and (c) C10A annealed in air at selected time and temperature conditions (labeled).

second low-angle peak does not form as in the case of the organically modified clays, the full width at half-maximum (FWHM) is found to increase from 1.6 to 2.3° due to a reduction in grain size and/or platelets containing populations of either Na⁺ cations or protons in the galleries.

The XRD patterns acquired from C15A and C10A annealed ex situ in air (panels b and c in Figure 4, respectively) exhibit contrasting results compared to those observed for the in situ samples heated in sealed capillaries. A new low-angle peak at $\sim 2.7^\circ$ 2θ develops upon ex situ heating of C10A for 12 days at 105 °C. Annealing at 160 °C also induces the formation of a small peak at 2.7° , in addition to a major peak at 6° 2θ , which implies significant collapse of the clay galleries. Ex situ annealing of C15A initially results in a sharpening of the low-angle peak, but a coinciding shift to larger d -spacing is not observed. The different XRD signatures generated by ex situ annealing C10A and C15A can be understood by considering the difference in relative volatilities among alkane and aromatic (toluene) decomposition products. Degradation of the organic surfactant is envisaged to first proceed by breaking the C–N bond to yield toluene and HT chains. The HT chains

subsequently cleave at the $\text{CH}_2\text{—CH}_2$ bonds to yield short-chain alkane molecules. Octane and shorter-chain alkanes have normal boiling points between -161 and 126 °C, whereas toluene boils at ~ 110 °C. Ex situ XRD suggests that free toluene persists in the interlayer galleries, requiring higher temperatures and longer times to diffuse out from the primary particles into the atmosphere. The alkanes, on the other hand, are generally more volatile and encounter less resistance (evidenced by the initially larger d -spacing of C15A relative to C10A) as they diffuse from the galleries. These organic vapors are trapped in the sealed capillaries used in conjunction with the in situ XRD experiments and eventually reach an equilibrium partition inside and outside the clay particles. Although the ex situ XRD experiments possess the same initial concentration difference (high alkane concentration inside the galleries and a negligible concentration outside), the organic vapors escape into the atmosphere upon diffusing from the clay, thereby preventing the concentration buildup needed to maintain vapor intercalation within the galleries. Yoon et al.¹³ have observed that C15A annealed in air at 250 °C for <10 min yields a d -spacing increase. At longer times, however, they report platelet collapse. In light of our results, we propose that at early times, the light alkanes generated upon degradation of the surfactant serve to increase the d -spacing, but prolonged high-temperature annealing (>10 min) promotes diffusion of these species out of the silicate galleries into the atmosphere and, consequently, a reduction in d -spacing.

Closer examination of Figure 4b provides insight into the effect of annealing C15A in air at both 105 and 160 °C. Exposure of C15A to 105 °C for 12 days (not shown in the figure) does not discernibly alter the XRD pattern from that of the pristine clay, and the two peaks positioned at 2.76 and $7.22^\circ 2\theta$ (3.20 and 1.22 nm, respectively) remain intact. However, further annealing (33 days) at this temperature shifts both peaks to smaller d -spacings (2.86 and 1.19 nm, respectively) due to degradation of the HT chains and loss of the resultant vapors from the silicate galleries. Such delayed changes under isothermal conditions are not uncharacteristic of molecular-level processes involving clay degradation, because TGA performed²³ on polypropylene (PP) NCs in air shows evidence of weight loss between 230 and 250 °C upon temperature ramping, whereas isothermal analysis at 200 °C reveals substantial weight loss after an induction period of only ~ 5 min. Exposure of C15A to a higher temperature (160 °C) for 12 days initiates collapse of the platelets, as evidenced by the low-angle peak shifting to $2.89^\circ 2\theta$ (3.05 nm). Further annealing at 160 °C collapses the platelets until only a single peak at $6.77^\circ 2\theta$ (1.30 nm) remains after 39 days. This corroborates our earlier FTIR results indicating that complete degradation of C15A occurs after exposure to 160 °C for 39 days because of the disappearance of CH_2 and other hydrocarbon vibrations. Qualitative comparison of the XRD patterns collected after 33 days at 105 and 160 °C reveals a significant temperature effect on platelet morphology. It is interesting that the XRD pattern obtained from C15A after exposure to 200 °C for only 0.2 h is consistent with an intermediate extent of

decomposition relative to that observed after 33 days at 160 °C, suggesting the existence of a time—temperature relationship.

Figure 4c confirms the existence of an initial scattering reflection at $4.57^\circ 2\theta$ (1.93 nm) in C10A. The low-intensity shoulder observed between 2.65 and 3.50 nm in Figure 3b is, however, much less pronounced because of the lower intensity of the copper tube vs the synchrotron X-ray source. Annealing C10A in air at 105 °C for 12 days appears to be sufficient enough to broaden the original reflection (the FWHM increases from 0.6 to 1.9°) and produce a new low-angle peak at $\sim 2.8^\circ$ (3.15 nm). In sharp contrast, exposure of C10A to 160 °C for the same time effectively degrades all the surfactant and generates either collapsed platelets at $6.05^\circ 2\theta$ (1.46 nm) or intercalated platelets at $\sim 2.8^\circ 2\theta$ (3.15 nm). Further annealing at this temperature reveals that the FWHM of the high-angle peak does not appreciably change (from 0.7°), but the low-angle reflection broadens considerably, which is consistent with structural breakdown. The morphology of C10A as assessed by XRD therefore appears much more susceptible to thermal oxidative degradation than that of C15A, although coloration changes are more pronounced for C15A (black) relative to C10A (gray) at comparable exposure times. The increased thermal susceptibility of C10A vs C15A is consistent with its lower onset degradation temperature (144 vs 180 °C) according to TGA.

As discussed previously, in situ XRD patterns for extruded NC17 without further heat treatment (see Figure 3c) exhibit an intercalated morphology, which is unstable due to thermal decomposition. The degraded alkyl surfactant chains produced during extrusion intercalate and swell the silicate galleries, thereby increasing the d -spacing. The high extrusion pressure and lack of a concentration driving force minimize diffusion of alkyl chains out of the interlayer. The extrudate rapidly cools upon emerging from the die and locks the alkane molecules in the interlayer. Although subsequent diffusion of such species through the PS matrix occurs, the process is expected to be slow because of the glassy nature of PS at temperatures below its T_g . Interlayer swelling during extrusion can be considered similar in principle to adding excess surfactant during cation exchange,^{28–32} but the swelling agents during cation exchange are not anticipated to volatilize to any appreciable extent below 200 °C (unlike the intercalated species in the extruded NCs). Ex situ XRD performed on extrudate strands confirms a modest increase in d -spacing relative to C15A. However, melt-pressing or annealing the extrudate above its T_g for a few minutes allows the d -spacing to approach that of neat C15A, which is indicative of an immiscible NC. On the basis of the scenario portrayed above, a suitable explanation for this observation is that annealing provides the thermal energy and time

(28) Hyun, Y. H.; Lim, S. T.; Choi, H. J.; Jhon, M. S. *Macromolecules* **2001**, *34*, 8084.

(29) Ho, D. L.; Briber, R. M.; Glinka, C. J. *Chem. Mater.* **2001**, *13*, 1923.

(30) Xi, Y. F.; Ding, Z.; He, H. P.; Frost, R. L. *J. Colloid Interface Sci.* **2004**, *277*, 116.

(31) Xi, Y.; Martens, W.; He, H.; Frost, R. L. *J. Therm. Anal.* **2005**, *81*, 91.

(32) Lee, S. S.; Lee, C. S.; Kim, M. H.; Kwak, S. Y.; Park, M.; Lim, S.; Choe, C. R.; Kim, J. J. *Polym. Sci., Part B: Polym. Phys.* **2001**, *39*, 2430.

necessary for the alkane chains to diffuse out of the interlayer, through the molten PS matrix and into the atmosphere. Except for the added diffusion through PS, this process is physically similar to that of C15A annealed ex situ. Other hybrid systems, such as a ternary NC composed of PP-g-maleic anhydride and PP prepared by twin-screw extrusion, have likewise been shown to be thermally unstable.³³

Anisotropic Orientation. Regarding diffraction studies of clay-induced polymer NCs, it is worthwhile to point out the impact of preferred orientation on observed diffraction patterns. Prior studies have repeatedly documented that MMT and OM-MMT platelets align parallel to the injection or extrusion direction for polyamide (PA),^{34–41} maleated-polyethylene (PE),^{42,43} maleated-PP,⁴³ and poly(vinyl chloride)⁴⁴ NCs. Preferred platelet orientation has also been observed in poly(*l*-lactide)⁴⁵ and poly(ϵ -caprolactone)⁴⁶ NCs prepared by solution intercalation wherein most of the platelets orient with their surface normal perpendicular to the film surface. In electrospun nylon NCs, the platelets align along the fiber direction.⁴⁷ Morgan and Gilman⁷ have provided an excellent comparative study of XRD and transmission electron microscopy (TEM). Because solid samples may yield misleading results due to preferred platelet orientation, they recommend using powder samples for detailed morphological analysis. Preferred orientation can also be induced, however, by specimen preparation of powder samples as the powder is pressed onto flat specimen holders. Varying the incidence angle of the X-rays with respect to the sample plate can be used to assess if the clay platelets preferentially pack parallel to the specimen holder surface. Varlot et al.³⁶ have examined PA NC films generated via extrusion–injection by rotating the films relative to the incident beam. The resultant XRD patterns differ substantially depending on position. Vermogen et al.⁴⁸ have proposed a statistical TEM methodology to ascertain factors that can lead to false XRD interpretations. While Vaia and Liu⁴⁹

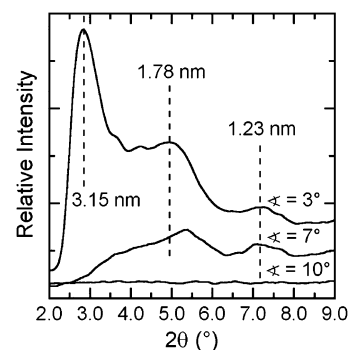


Figure 5. XRD patterns ($\lambda = 0.154$ nm) demonstrating the preferred orientation of C15A platelets in a flat NC17 film tested in reflectance at three different incidence angles (labeled).

provide a detailed overview of XRD performed in reflection using the Bragg–Brentano parafocusing geometry, the influence of incidence angle on XRD analysis of polymer NCs remains a largely unexplored topic.

Undesirable effects of preferred platelet orientation can almost be completely precluded by placing a sample into a rotating capillary and measuring the diffraction in transmission. When using reflection to explore the extent of preferred orientation in a film of NC17 taped to an aluminum plate sample holder; however, we find that rotation of the sample holder by a mere 4° results in extinction of the lowest-angle peaks and rotation by 7° yields complete extinction of all peaks, as shown in Figure 5. Thus, the clay platelets appear to be well-aligned within the polymer after melt processing. Interestingly, markedly less alignment is observed in the NC7 film for which extinction of the lowest-angle reflection is not observed until the incident angle is rotated by more than 12° . Platelet aggregates in NC17 align to a greater extent along the extrusion direction because of the higher clay concentration and thus exhibit a narrower distribution of orientation angles. Small- and wide-angle X-ray scattering studies⁵⁰ of PE/OM-MMT NCs extruded into films provide evidence that aggregates are highly oriented with their surface normal aligned perpendicular to the extrusion direction. In similar NCs prepared with native MMT, such aggregates appear smaller with the platelets remaining randomly oriented in the films. Investigations of maleated-PP^{42,43} and maleated-PE⁴³ have likewise demonstrated that larger aggregates or higher clay concentrations possess more highly oriented platelets. Collapsed aggregates (exhibiting diffraction peaks at high 2θ) are responsible for XRD reflections observed over a greater range of incidence angles because the platelets are less likely to be aligned along the extrusion direction. Similarly, disappearance of scattering reflections discerned from neat clay can occur at very low incidence angles (5°) due to alignment of the platelet normals perpendicular to the surface of the specimen holder.

C. Macromolecular Characteristics. In the previous sections, we have examined the effect of extended thermal treatment on the chemical and morphological characteristics of three MMT-based clays and PS NCs fabricated from

- (33) Reichert, P.; Hoffmann, B.; Bock, T.; Thomann, R.; Mülhaupt, R.; Friedrich, C. *Macromol. Rapid Commun.* **2001**, *22*, 519.
 (34) Kojima, Y.; Usuki, A.; Kawasumi, M.; Okada, A.; Kurauchi, T.; Kamigaito, O.; Kaji, K. *J. Polym. Sci., Part B: Polym. Phys.* **1994**, *32*, 625.
 (35) Kojima, Y.; Usuki, A.; Kawasumi, M.; Okada, A.; Kurauchi, T.; Kamigaito, O.; Kaji, K. *J. Polym. Sci., Part B: Polym. Phys.* **1995**, *33*, 1039.
 (36) Varlot, K.; Reynaud, E.; Kloppfer, M. H.; Vigier, G.; Varlet, J. *J. Polym. Sci., Part B: Polym. Phys.* **2001**, *39*, 1360.
 (37) Masenelli-Varlot, K.; Reynaud, E.; Vigier, G.; Varlet, J. *J. Polym. Sci., Part B: Polym. Phys.* **2002**, *40*, 272.
 (38) Tidjani, A.; Wald, O.; Pohl, M.-M.; Hentschel, M. P.; Bernhard, S. *Polym. Degrad. Stab.* **2003**, *82*, 133.
 (39) Yalcin, B.; Cakmak, M. *Polymer* **2004**, *45*, 2691.
 (40) Usuki, A.; Hasegawa, N.; Kato, M. In *Inorganic Polymeric Nanocomposites and Membranes*; Springer-Verlag: Berlin, 2005; Vol. 179, p 135.
 (41) Weon, J. I.; Xia, Z. Y.; Sue, H. J. *J. Polym. Sci., Part B: Polym. Phys.* **2005**, *43*, 3555.
 (42) Koo, C. M.; Ham, H. T.; Kim, S. O.; Wang, K. H.; Chung, I. J.; Kim, D. C.; Zin, W. C. *Macromolecules* **2002**, *35*, 5116.
 (43) Koo, C. M.; Kim, S. O.; Chung, I. J. *Macromolecules* **2003**, *36*, 2748.
 (44) Yalcin, B.; Cakmak, A. *Polymer* **2004**, *45*, 6623.
 (45) Ogata, N.; Jimenez, G.; Kawai, H.; Ogihara, T. *J. Polym. Sci., Part B: Polym. Phys.* **1997**, *35*, 389.
 (46) Jimenez, G.; Ogata, N.; Kawai, H.; Ogihara, T. *J. Appl. Polym. Sci.* **1997**, *64*, 2211.
 (47) Fong, H.; Liu, W. D.; Wang, C. S.; Vaia, R. A. *Polymer* **2002**, *43*, 775.
 (48) Vermogen, A.; Masenelli-Varlot, K.; Seguela, R.; Duchet-Rumeau, J.; Boucard, S.; Prele, P. *Macromolecules* **2005**, *38*, 9661.

(49) Vaia, R. A.; Liu, W. D. *J. Polym. Sci., Part B: Polym. Phys.* **2002**, *40*, 1590.

(50) Bafna, A.; Beaucage, G.; Mirabella, F.; Mehta, S. *Polymer* **2003**, *44*, 1103.

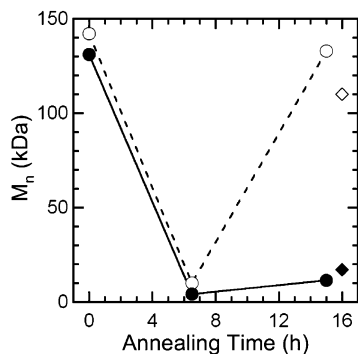


Figure 6. Comparison of time-dependent M_n values calculated from MALS (open symbols, dashed lines) and the PS universal calibration (filled symbols, solid lines) for neat PS (○, ●) and NC7 (◇, ◆) after exposure to 250 °C in an O_2 -rich environment.

C15A. Here, the effects of extrusion and long-time quiescent annealing on PS molecular weight at 250 °C in an O_2 -rich environment are explored. Changes in molecular weight are minimal when annealed under N_2 and are not shown for that reason. Extrusion of PS containing C15A (NC7 or NC17) results in the formation of a stable immiscible NC with long PS chains residing along the periphery of the silicate sheets, thereby preventing significant chain diffusion into the galleries.^{51,52} At temperatures above 220 °C, thermal-oxidative chain scission preferentially occurs in close proximity to the clay and is responsible for cleaving adsorbed PS chains. Shortened chains originating from chains along the silicate edges or within the bulk successfully penetrate into the C15A galleries, as evidenced by simultaneous increases in d -spacing and elastic modulus. Figure 6 shows the molecular weight of neat PS (M_n , calculated using a universal calibration and MALS) as a function of annealing time in an O_2 -rich environment at 250 °C. Results obtained from both techniques are comparable up to 7 h and verify that the PS molecular weight decreases considerably with increasing annealing time. At 14 h, the value of M_n computed using the universal calibration remains comparable to that evaluated at 7 h. In sharp contrast, however, the value of M_n discerned from MALS increases dramatically and approaches the molecular weight of the pristine PS. Similar trends are observed for M_w , as well as for both NC7 and NC17, in which case only the value of M_n ascertained for NC7 after 16 h at 250 °C in an O_2 -rich environment is shown for comparison in Figure 6.

Signals acquired from MALS and differential refractive index (DRI) for neat PS before and after annealing for select times in an O_2 -rich environment at 250 °C are provided in Figure 7a. Both initial signals display maxima at an elution volume of 10.0–10.5 mL, followed by a precipitous drop in the DRI signal at ~20 mL, which is attributed to coelution of solvent and polymer. Exposure to an O_2 -rich environment at 250 °C results in several signal changes. The maxima in the MALS and DRI signals shift to larger elution volumes, with the shift in the DRI signal being more pronounced than the MALS signal because DRI is based on the number of

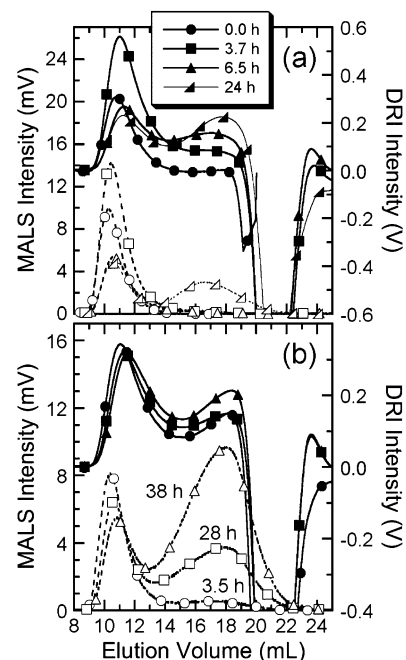


Figure 7. Complementary MALS (open symbols, dashed lines) and DRI (filled symbols, solid lines) signals for (a) PS and (b) NC7 after annealing at different times (see legend or labels) in an O_2 -rich environment at 250 °C.

molecules and is therefore more sensitive to chain scission. A second maximum develops and grows in both signals (only after 24 h according to MALS) at larger elution volumes, and corresponds to shortened PS chains resulting from thermal oxidative chain scission. It should be noted that this peak does not form when the PS is annealed in an O_2 -rich environment below 220 °C or in inert environments at all temperatures considered in this study (up to 250 °C). Last, the area ratio discerned from the small- to large-elution-volume peaks decreases with increasing exposure time, signifying that an increasingly large population of compact chains is produced. The trends for NC7 in Figure 7b resemble those for neat PS in Figure 7a. Longer treatment times are included in Figure 7b to provide perspective on the growth of the larger-elution-volume peak in the MALS signal. The overall and individual peak molecular weights determined by MALS and DRI for both neat PS and NC7 are reported in Table 1. The molecular weights of NC7 after extrusion are lower than those of pristine PS, but commensurate with those of extruded PS. After 3.5 h, the DRI signal obtained from NC7 develops a larger elution peak similar to that of neat PS. Although some discrepancy in the molecular weights listed in Table 1 may be ascribed to instrumental limitations, another consideration here is the reduced diffusion length of free radicals in NC7 due to the higher melt viscosity and more tortuous pathway established by the impermeable clay platelets. It is reasonable to expect that free radicals generated during scission may attack the same chain in NC7, resulting in shorter chains in NC7 than in PS. The number of chains degraded in NC7 is, however, expected to be lower if the number of free radicals is comparable in both systems. Within the context of this scenario, M_n will be higher and M_w will be lower for NC7 relative to neat PS under identical conditions.

(51) Frankowski, D. J.; Spontak, R. J.; Khan, S. A. manuscript in preparation for submission.

(52) Frankowski, D. J.; Khan, S. A.; Spontak, R. J. *Adv. Mater.* **2007**, in press.

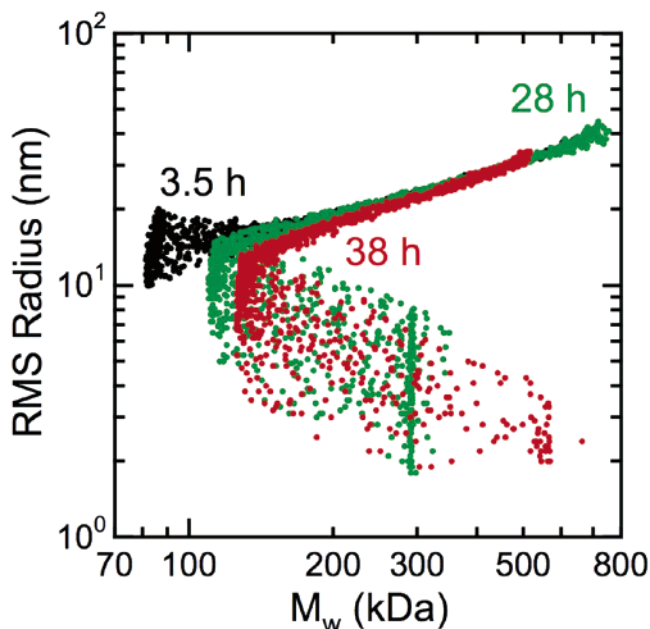


Figure 8. Abnormal elution behavior indicative of PS branching or other nonlinear molecular architectures in NC7 after prolonged annealing times of 3.5 (black), 28 (green), and 38 h (red) in an O_2 -rich environment at 250 °C.

This sequence of molecular-level events is consistent with our proposed scission-intercalation mechanism: chains residing along the periphery of the clay tactoids preferentially undergo chain scission and long PS chains subsequently replace degraded short chains as the latter diffuse into and intercalate the clay galleries. After annealing NC7 for at least 28 h at 250 °C, the relative area of the larger- to smaller-elution-volume peaks becomes clearly pronounced in the MALS signal in Figure 7b. If linear PS chains constitute scission products, then the chains eluting after the first maximum would be of reduced molecular weight. The DRI signal should, however, be sensitive to the number of chains and would be expected to grow faster than the MALS signal. These conflicting MALS and DRI traces can be resolved by recognizing that high-molecular-weight chains do not always elute first. Podzimek and co-workers^{53–55} have previously demonstrated that such abnormal elution behavior can reflect branching and cross-linking. To determine the extent of nonlinear chains generated, we plotted the rms chain radius (R) in Figure 8 as a function of M_w . Data points acquired after 3.5 h show the expected trends wherein R increases with increasing M_w and the corresponding scaling exponent is 0.5 (i.e., $R \approx M_w^{1/2}$). This result is consistent with Gaussian coils composed of linear chains. After annealing for 28 h, R in the vicinity of 1×10^5 Da does not scale with M_w and, in fact, becomes highly degenerate (several R values exist for a given value of M_w). This deviation from typical behavior becomes increasingly more pronounced as the annealing time is increased further to 38 h. Similar results have been previously documented for highly branched^{53,56,57} and star⁵⁸

polymers, dendrimers,⁵⁹ and brushes.⁶⁰ Thus, the fast growth of the maximum at larger elution volume observed by MALS is attributed to the development of branched PS chains with a reduced hydrodynamic size that are detected at later elution times by both MALS and DRI.

Provided below is a summary of operational mechanisms as the present PS NCs are exposed to extended high-temperature annealing in an oxidative environment. The PS chains initially undergo chain scission to yield similar MALS results, but a second peak identified by DRI arises at larger elution volumes. At intermediate annealing times (10–25 h), PS continues to undergo chain scission, which competes with intermolecular radical transfer and termination by recombination because the number of radicals increases. The increased viscosity^{61,62} and confinement⁶³ of PS chains due to intercalation of shortened chains under these conditions also enhances radical recombination. Figure 8 proves that the increased intensity of the maximum observed at larger elution volume is not due to the formation of linear chains with reduced molecular weight, but rather to branched molecules with M_w values ranging from 100 to 300 kDa. After annealing for 38 h, the lowest M_w identified has increased, further signifying that the molecular weight of the branched polymers has likewise increased. These time- and temperature-dependent processes strongly influence other material characteristics, such as the d -spacing of the silicate sheets and the elastic modulus of the NC. It is intriguing that the rates by which the d -spacing and modulus increase slow down after prolonged annealing. This observation may result from (i) the NC approaching thermodynamic equilibrium so that the driving force for intercalation gradually diminishes, or (ii) generation of sufficiently branched chains that hinder continued diffusion of PS chains into the interlayers. Acidic sites on the clay surface can likewise catalyze PS cross-linking, as previously demonstrated for NCs consisting of poly(styrene-*co*-acrylonitrile)⁶⁴ or PP.⁶⁵ Once the chains are intercalated in the clay galleries, they are more likely to contact these active sites and undergo cross-linking, which may also explain the reduced rate of intercalation at long thermal treatment times and the apparent crossover from predominately chain scission to branching and cross-linking.

IV. Summary

Polymeric NCs prepared with organically modified clays are routinely exposed to elevated temperatures during either

(53) Podzimek, S.; Vlcek, T.; Johann, C. *J. Appl. Polym. Sci.* **2001**, *81*, 1588.

(54) Podzimek, S.; Vlcek, T. *J. Appl. Polym. Sci.* **2001**, *82*, 454.

(55) Podzimek, S. *J. Appl. Polym. Sci.* **1994**, *54*, 91.

(56) Cheng, G. L.; Simon, P. F. W.; Hartenstein, M.; Muller, A. H. E. *Macromol. Rapid Commun.* **2000**, *21*, 846.

(57) Sarbu, T.; Lin, K. Y.; Ell, J.; Siegwart, D. J.; Spanswick, J.; Matyjaszewski, K. *Macromolecules* **2004**, *37*, 3120.

(58) Frater, D. J.; Mays, J. W.; Jackson, C. *J. Polym. Sci., Part B: Polym. Phys.* **1997**, *35*, 141.

(59) Percec, V.; Ahn, C. H.; Cho, W. D.; Jamieson, A. M.; Kim, J.; Leman, T.; Schmidt, M.; Gerle, M.; Moller, M.; Prokhorova, S. A.; Sheiko, S. S.; Cheng, S. Z. D.; Zhang, A.; Ungar, G.; Yearley, D. J. *P. J. Am. Chem. Soc.* **1998**, *120*, 8619.

(60) Gerle, M.; Fischer, K.; Roos, S.; Muller, A. H. E.; Schmidt, M.; Sheiko, S. S.; Prokhorova, S.; Moller, M. *Macromolecules* **1999**, *32*, 2629.

(61) Mita, I.; Horie, K. In *Degradation and Stabilization of Polymers*; Jellinek, H. H. G., Ed.; Elsevier: New York, 1983; Vol. 1, p 235.

(62) McNeill, I. C.; Zulfikar, M.; Kousar, T. *Polym. Degrad. Stab.* **1990**, *28*, 131.

(63) Jang, B. N.; Wilkie, C. A. *Polymer* **2005**, *46*, 2933.

(64) Jang, B. N.; Wilkie, C. A. *Polymer* **2005**, *46*, 9702.

(65) Qin, H. L.; Zhang, S. M.; Zhao, C. G.; Hu, G. J.; Yang, M. S. *Polymer* **2005**, *46*, 8386.

fabrication or application, which can have a significant impact on structure and properties. To address this issue in systematic fashion and resolve conflicting reports in the literature, we have employed FTIR spectroscopy, XRD, and SEC to investigate the thermal stability of three pristine MMT clays (one native and two modified), the polymer matrix, and two corresponding NCs generated by melt extrusion. The two OM-MMTs show evidence of alkyl surfactant degradation at temperatures as low as 105 °C in air. Annealing at higher temperatures (160 °C) increases the rate of degradation and initiates the loss of aromatic moieties and aliphatic chains. After 39 days of being annealed in air at 160 °C, the organic surfactants are completely degraded because of the absence of various CH₂ absorption modes that would be present if the aliphatic chains were present. This result is consistent with ex situ XRD, which shows no diffraction peaks corresponding to the *d*-spacing(s) of the initial modified clays. The native MMT, on the other hand, is significantly more stable than either OM-MMT, each of which exhibits diffraction peaks at both low and high 2θ . The low-angle peak is believed to correspond to platelets with aliphatic and/or aromatic moieties located inside the platelet galleries, whereas the high-angle peak most likely identifies platelets with incomplete cation exchange. Variable-temperature in situ XRD of the OM-MMTs in sealed capillaries reveal platelet collapse, as well as platelet expansion due to intercalation of organic vapors generated

from thermal decomposition, with increasing temperature. Ex situ annealing of these clays yields different results due to escape of volatile organics to the atmosphere. The extruded NCs possess an increased, although unstable, *d*-spacing relative to the pristine clay due to intercalation of short aliphatic chains from degraded C15A. Subsequent thermal treatment permits intercalated vapors to diffuse from the NCs and reduce the *d*-spacing to that of the parent OM-MMT. Annealing the NCs in O₂-rich environments above 220 °C promotes chain scission of PS and allows small chains to intercalate into the clay galleries. After ~10 h, however, PS chains become branched and cross-linked because of intermolecular reactions, which may account for the apparent reduction in the rate of intercalation, as discerned by both XRD and dynamic rheological measurements.⁵¹

Acknowledgment. This study was supported by the STC Program of the National Science Foundation under Agreement CHE-9876674. We thank Dr. Isaac LaRue formerly of the University of North Carolina at Chapel Hill and now at Stetson University for the SEC measurements based on the universal calibration. Synchrotron X-ray diffraction conducted at beam line X7b at BNL-NSLS was supported by Contract DE-AC02-98CH10086 with the U.S. Department of Energy, Office of Basic Energy Sciences, Division of Chemical Sciences. The NSLS is supported by the Divisions of Materials and Chemical Sciences of the Department of Energy.

CM061953K